Electron transfer in keV-energy $^4He^{++}$ atomic collisions. I. Single and double electron transfer with He, Ar, H_2, and N_2 †

J. E. Bayfield and G. A. Khayrallah
J. W. Gibbs Laboratory, Physics Department, Yale University, New Haven, Connecticut 06520
(Received 24 June 1974)

Single- and double-electron-transfer cross sections have been measured for a $^4He^{++}$ beam incident on thin He, Ar, H_2, and N_2 gas targets over the energy range 15–125 keV. Comparison with previous $^3He^{++}$ experimental results is made at the same incident particle velocity. For He^{++} collisions with He, we find good agreement with the theory for double electron transfer, but conclude that the single-electron-transfer cross section is far from being understood. Interpretation of the data in terms of simple theoretical ideas indicates that capture into excited states of the He^+ ion can be the dominant single-electron-transfer process in some keV-energy He^{++} atomic collisions.

I. INTRODUCTION

In recent years considerable interest has developed in electron-transfer collisions of highly ionized ions with atoms and molecules. Some of this interest lies in a number of possible applications. For those cases where the collision system contains few electrons, tests of theoretical predictions are possible. A common feature of these processes is a long-range Coulomb repulsion of the ions in the final state, with consequences not yet well understood.

A prototype collision system with total charge greater than 1 is that of He^{++} incident upon some neutral atom or molecule. The effort to understand such processes contributes to studies of certain high-temperature systems such as the sun, solar wind, and fusion reactors. As one possibility of fueling a reactor is by injection of ^3He, the various electron-transfer (both pick-up and stripping) cross sections need to be known for wide ranges of collision energy and choice of target atom. Not only are these processes useful for the production of beams for injection into mirror machines, but once an He^{++} is in the plasma, electron transfer processes involving H, D and He are of importance in particle and energy loss from the plasma.

For the one-electron He^{++}-H and two-electron He^{++}-He systems a number of theoretical cross-section calculations are available for the various possible electron-transfer channels. In the case of single-electron transfer in these systems a considerable production of the excited states of He^+ is predicted. This concurs with the observation that the energy defect involved in transfer into the 1s state is going to be large simply because the $He^+(1s)$ ionization potential is much greater than that of any first-ionization potential of any neutral atom or molecule. Hence the experimental determination of the final electronic states in such processes is of great importance both in testing theory and in a number of applications. The needed accuracy in some cases is ± 20%. The following two papers II and III will describe our experiments on the formation of $^4He^+(2s)$ in $^4He^{++}$-H, $^4He^{++}$-^4He, and other $^4He^{++}$ collisions.

It is clear from the history of experimental studies of proton collisions with various atoms and molecules that unknown systematic error of the order ± 50% or more often exists in published electron-transfer cross-section data. Only after the completion of a large number of independent experiments have a few standard cross sections been determined to about ± 10%, such as the overall or "total" single-electron-transfer cross section σ_{10} in H^+-H_2 collisions. For incident helium ions similar precision exists only for $^4He^+$ collisions, in particular for σ_{10} with the target atom $^4He^0$. The few past lower-keV-energy He^{++} experiments have employed incident $^3He^{++}$ beams to avoid the mass resolution needed to prepare a $^4He^{++}$ beam free from H_2^+ contamination. In the case of He^{++} – H, past cross-section values for incident $^3He^{++}$ are traced through a chain of relative measurements back basically to σ_{10} for $H^+ - H_2$, a procedure having a number of associated uncertainties such as relative detector efficiencies for H and He particles and the resettability of experimental conditions as one switches from one incident ion beam to the other. The present series of experiments always works within the ^4He system and involves relative measurements ultimately based on σ_{10} for $^4He^+ - {}^4He$.

The comparison of the results of this paper with available $^3He^{++}$ data can then be interpreted in one of two basic ways: as an additional effort towards finding a standard cross section for He^{++} collisions or as a search for possible residual isotope effects on the cross section when plotted as

a function of relative velocity of the two collision partners. We shall see that the former interpretation is more useful at the present time because of discrepancies in the $^3He^{++}$ data, and that a standard He^{++} cross section is badly needed to help resolve some serious discrepancies in the He^{++}-H data, as discussed in paper III.

This paper (I) begins with a description in Sec. II of our apparatus, with emphasis on the techniques and test procedures associated with using a pure $^4He^{++}$ beam. Sec. III presents our results and conclusions. We have reported preliminary results for the present experiments at the eighth ICPEAC meeting.[1]

II. APPARATUS

A. General description

A schematic diagram of the apparatus used in the present study is shown in Fig. 1 along with a figure caption describing the individual components.

A high-power radio-frequency ion source "A" was used to produce He^{++} particles. An oscillator "B" supplied the radio-frequency power to the source discharge. A series of electrostatic tube lenses "C" focused and accelerated the beam to its final energy. The beam was then positioned by parallel plates "D," gated by parallel plates "E," and mass analyzed by the 60° bending magnet "F." The beam was then passed through four circular apertures of diameter 0.063 cm each; the first, "G," was placed just outside the analyzing magnet, the second and third were the entrance and exit apertures of an unused second scattering target "I," and the fourth aperture was located at the entrance of the scattering target "K." The first and last of these apertures helped limit the phase space occupied by the incident beam. The sets of plates "H" and "J" helped position the beam. The different charge components of the beam were electrostatically separated with a pair of parallel plates "L." The charged components of the beam were collected by biased Faraday cups "M" and "N," while the neutral-beam component was collected by the secondary-electron-emission neutral-beam Faraday cup "O." Cup "O" was removable from the beam path. At the end of the machine a translatable detection assembly "P" scanned the beam. Section II D describes this assembly in detail.

The experiment was performed in a bakeable ultrahigh vacuum system with base pressures of the order 2×10^{-9} Torr. Differential pumping apertures and tubes, marked "X" in Fig. 1, helped isolate the separately pumped regions of the vacuum system. Details of the vacuum system, scattering target assembly, and the accelerating region have been described.[2]

The entire room containing the machine was lined by a coil to provide cancellation of the vertical component of the Earth's magnetic field. A smaller coil cancelled the horizontal nonaxial (relative to the machine axis) component of the Earth's magnetic field in the drift region between the charge-analysis region and the translatable-detector region.

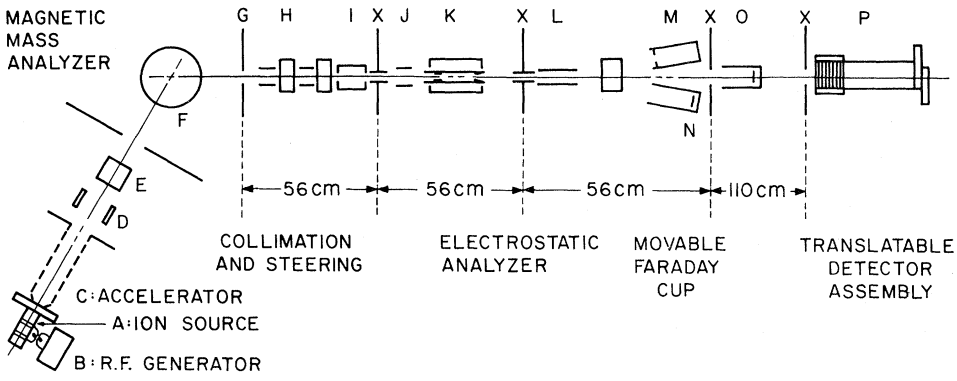

FIG. 1. Apparatus. A: Radio-frequency discharge ion source; B: radio-frequency oscillator, 125 MHz, 400 W; C: electrostatic accelerating and focusing electrodes; D: ion-beam positioning plates; E: ion-beam gating plates; F: 60° circular pole-piece magnetic momentum analyzer; G: ion-beam collimating aperture, 0.063-cm diameter; H: ion-beam positioning plates; I: additional apertures, 0.063-cm diameter; J: ion-beam positioning plates; K: scattering-target, with its entrance aperture of 0.063-cm diameter serving as a final beam collimating aperture; L: electrostatic charge-analyzing parallel plates; M: positive-ion-beam monitoring Faraday-cup assembly; N: negative-ion-beam monitoring Faraday-cup assembly; O: secondary-electron-emission neutral-beam detector; P: translatable detection assembly with a circular entrance aperture of diameter 0.025 cm.

B. Ion beam

1. Ion source operation

The radio-frequency ion source used was an ORTEC Model 321 source modifed by us to include a tungsten extraction tip. An oscillator operating at 125 MHz and with a nominal power input of 400 W supplied radio-frequency power to the discharge. The oscillator output was link-coupled to two circular rings that surrounded the quartz ion-source bottle, see Fig. 2.

Two source plasma modes (and sometimes more) were found: a very optically bright green mode as well as a dim mode at intermediate magnetic-field settings. The dim mode produced much more He^{++} beam than the bright mode. A current of 0.35 A through the magnet coil was sufficient for operation in the dim mode. The extraction voltage was found to be least dramatic in influencing the output current, and a relatively low value of 1800 V was used to conserve the lifetime of the ion source.

2. Ion beam

After being deflected by the mass-analyzing magnet, the $^4He^{++}$ beam was collimated and then entered the target with a nominal diameter of 0.063 cm and a nominal angular spread of 0.065° full width at half-maximum (FWHM). The running intensity of the $^4He^{++}$ beam after this collimation was larger than 10^{-10} A. About 99.5% of the original He^{++} beam phase space was discarded by the very tight collimation needed to increase the resolving power of the 60° magnetic-analysis system as well as to facilitate angular-distribution studies of scattered particles.

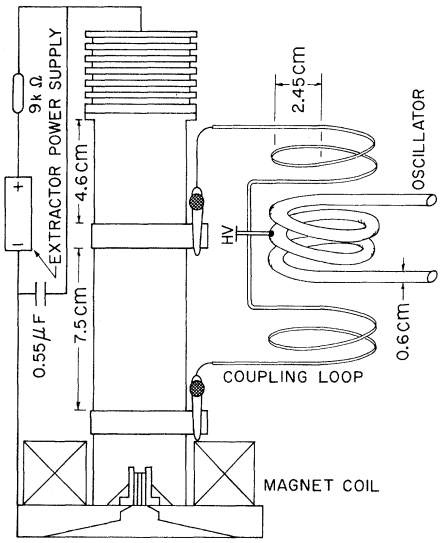

FIG. 2. Schematic diagram of the ion source and the inductive coupling loops.

The production of $^4He^{++}$ was complicated by the almost identical mass-to-charge ratios of $^4He^{++}$, H_2^+, and D^+. Purity of the ion-source gas supply was not enough to stop possible contamination, as H_2^+ could be generated in the ion-source bottle itself via many mechanisms. For example, some dissociation of large hydrocarbon molecules could have occurred by sputtering of the vinyl-acetate vacuum seals. (Quantities of C^+ and O^+ were occasionally observed in the output mass spectra from the ion source.) The natural abundance of deuterium relative to hydrogen is very small (~0.015%), and no deuterium was used in the system. Therefore, the following discussion will concentrate on possible H_2^+ contamination only.

The mass of $^4He^{++}$ is unequal to the mass of H_2^+ primarily because of differences in the binding energies of their nuclei. The fractional mass difference is about $\Delta M/M \simeq \frac{1}{150}$. Hence when these two ions are accelerated by the same voltage, they have slightly differing velocities and momenta.

The present experiments employed high ion-beam mass resolution in order to directly separate $^4He^{++}$ from H_2^+. In fact, our lower useful beam-energy limit was set, in practice, by the increase in fractional energy spread of the beam with decreasing energy, which brought the two mass peaks (as observed by scanning magnetic-analyzer current or accelerator voltage) closer and closer together. A useful measure of the amount of overlap of the tails of the two mass peaks is a quantity called the visibility V,

$$V \equiv (I_{\max} - I_{\min})/(I_{\max} + I_{\min}),$$

where $I_{\min}$ is the value of the transmitted beam current at the minimum between the two peaks, and $I_{\max}$ is the maximum transmitted current of the smaller H_2^+ peak. At the lowest energy the visibility was at least 0.90 whenever data were taken. Considerably lower values were sometimes observed when ion-source conditions or accelerator focusing were not yet optimized.

Scattering experiments were used to directly determine the absolute contamination ratio of the $^4He^{++}$ beam intensity relative to that for H_2^+, with the analyzer magnet tuned to $^4He^{++}$. The fact was used that only H_2^+ dissociation could lead to protons at one half the energy of the H_2^+ ions. Such protons would be deflected at $\frac{1}{2}$ and $\frac{1}{4}$ the voltages needed to deflect the $(H_2^+, {}^4He^{++})$ and $^4He^+$ ions, respectively, as all these are traveling at the same velocity. Knowledge of a scattering target thickness Π, the intensity of the scattered proton beam, and the proton-production cross section[3]

made possible a calculation of the intensity of the H_2^+ incident-beam component. Except at our lowest beam energy, the fraction of H_2^+ in the main $^4He^{++}$ running beam never approached 0.2%. At 7 keV the value of 0.2% was obtained with a corresponding visibility of $V = 0.90$. This amount of contamination led to some small corrections to the 7-keV data and a somewhat larger over-all experimental uncertainty. At higher energies the effects of H_2^+ contamination were completely negligible.

The energy spread of the ion source was measured in two separate and distinct ways. In the first procedure, at fixed magnet-analyzer and accelerator-focus settings the accelerator voltage was increased through both $^4He^{++}$ and H_2^+ peaks. Bounds on the FWHM energy spread were determined from the voltage readings at half maximum of the beam-current intensity through the target. In the second method, the magnetic field required to pass the beam was calibrated as a function of the sum of the accelerating and ion-source extraction voltages. Then for fixed accelerator, extractor, and focus settings the magnet was scanned through both H_2^+ and $^4He^{++}$ beams, thus determining the combined beam momentum spread and inherent momentum resolution of the magnet-analyzing system. Figure 3 shows an example of a magnet scan. The bound on the energy spread was measured each way to be 30± 10 V FWHM. This value has contributions from (i) the "true" energy spread associated with collisions in the ion source, (ii) the resolution of the analyzer, and (iii) an induced radio-frequency modulation[4,5] of the energy of the beam characteristic of rf ion sources.

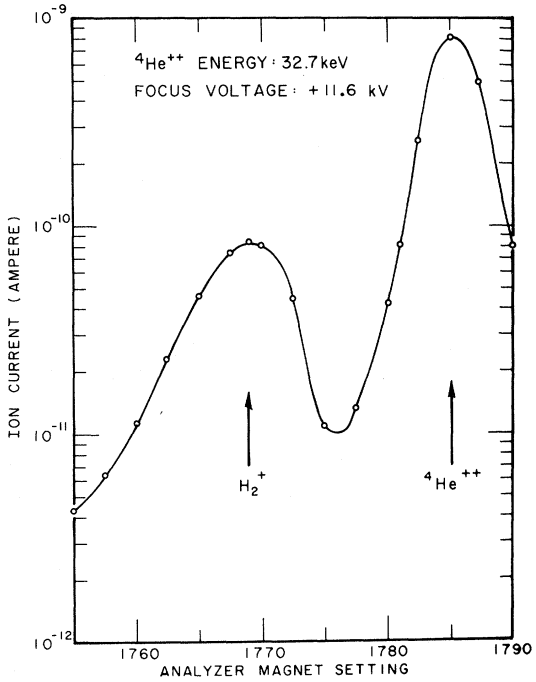

FIG. 3. Analyzer magnet scan of a 32.7-keV ($^4He^{++}$, H_2^+) beam. Total current passing through the scattering cell is plotted vs analyzer-magnet setting. These settings were proportional to the analyzer-magnet current and hence its magnetic field. It is seen that the two mass peaks of H_2^+ and $^4He^{++}$ are very well separated from each other. The visibility here is equal to 0.79.

C. Properties of the scattering target system

1. Scattering cell

Two interchangeable 10.2-cm-long gas cells were used. The first had a large vertical rectangular exit aperture, 0.203×0.76 cm, permitting angular-distribution measurements up to 3°. The entrance diameter of the conical shaped entrance aperture for this cell was 0.0254± 0.0013 cm. The second cell had a circular entrance aperture (also conical shaped for sharp "slit" edges) of diameter 0.063± 0.001 cm, and a circular exit aperture of diameter 0.25 cm that was observed to transmit all scattered particles at angles less than 0.75°. After angular distributions were measured using the first cell, the second cell was used for determining the total scattering cross sections reported here.

2. Target gas-handling system

The scattering-cell gas-handling system was manufactured from 304 stainless steel and was bakeable. The system could cycle three gases separately since it contained three separate ballast volumes that were connected to one gas feed line and one pumping manifold by a set of Viton-A O-ring pneumatic valves. The operation of these valves could be programmed and controlled to cycle through the gases in a predetermined fashion.

The whole assembly was pumped by a mercury diffusion pump supplemented by a thermoelectric baffle and a liquid-nitrogen trap. The pressure in the ballast volumes could be read by a Baratron capacitance manometer. The pressure used was usually set at 30 Torr, always four or more orders higher than the base pressure of the gas-handling system. Gas from the ballast volumes was fed to the target cell through a highly stable leak valve. A gas-bypass valve with a very large conductance short-circuited the leak-valve target combination, permitting the fixed gas flow (when desired) to pass directly to the main vacuum

chamber surrounding the target cell. This was an important "gas-dump" feature permitting the direct measurement of residual scattering due to gas outside the cell itself.[2]

3. Determination of scattering-target thickness

For a fixed leak-valve opening and a fixed gas-handling system ballast pressure, one absolute value of a target thickness Π was determined by performing an experiment on the single-electron-transfer process $^4He^+ + {}^4He \rightarrow {}^4He + {}^4He^+$. The total cross section for this process has been measured absolutely by many investigators and has the value 3.9 ± 0.2 Å^2 at 32 keV.[6-9] The energy dependence of this cross section was checked, with results in agreement with the published data. This calibration gave us $\Pi_{max} = 0.0137 \pm 0.0014$ atoms per Å^2 for He at the maximum ballast pressure used, and hence maximum flow rate and maximum target pressure. Owing to gas flow conservation this same Π arose when other gases were fed into the target at the same temperature and ballast pressure in the flow-limited gas-handling system, a feature checked through earlier cross-section measurements.[2,10]

The linear dependence of the scattering signals upon ballast pressure was checked by direct measurement of the derivative of signal dependence on pressure. This derivative was found to be independent of pressure except at the highest target pressures used, where it decreased by 5%.

Another independent determination of an absolute value of target thickness was made by using a 10-keV H_2^+ beam incident on Ar, H_2, N_2, and He targets and looking at the production of fast protons produced by dissociation. Cross sections for this have been measured by others a number of times with the value for He at 10 keV being 2.0 ± 0.4 Å^2.[3] This method determined $\Pi_{max} = 0.0124$ Å^{-2} for He to an accuracy of about ± 20%. The Π so obtained for the different gases agreed with that obtained above to within the accuracies of the measurements.

D. Translatable detection system

Figure 4 is a schematic diagram of the translatable detection assembly used for angular distribution studies and labeled "P" in Fig. 1. The beam entered the assembly through an interchangeable collimating circular aperture "Q" of minimum diameter 0.025 ± 0.0025 cm. This aperture had a 45° knife edge to reduce slit scattering. The electrostatic analyzer "R" separated the charged components of the beam so that simultaneously detector "U" could collect the neutral component, detector "T" could collect the singly-charged He^+ ions, and detector "S" could collect the incident He^{++} ions. The beam deflection angles were about 8° and 16° for detectors "T" and "S," respectively. The electrostatic deflector consisted of two plane-parallel plates of unequal deflecting length designed so that no positive He ion-beam component struck the plates. The Faraday cup "S" was designed and fabricated from nonmagnetic 314 stainless steel and had a 1.22-cm entrance aperture. About −100 V was applied to the front suppressor electrode of this cup to contain secondary electrons inside the cup. With collimator "Q" very large, the readings of Faraday cup "S" were compared with those of the precision Faraday cup[2] "M," with the observed currents agreeing to within a few percent up to 70-keV incident $^4He^{++}$ energy. This maximum comparison energy was limited by the high-voltage cables connected to the deflection plates "R." Detectors "T" and "U" were two Bendix Model M-306 resistive-strip magnetic multipliers. These were operated in both pulse-counting and d.c. current modes. The output pulses for the pulse mode were amplified by two stages of a fast-rise-time home-built (gain of 10 per stage) voltage-sensitive amplifier, discriminated, and counted by a 100-MHz scaler.

The two magnetic multipliers were arranged so that the magnetic field of one multiplier did not significantly affect the internal field of the other multiplier. (They were positioned antiparallel to each other.) Their fringe magnetic fields had a negligible effect on the ion-beam collection efficiencies.

The entire assembly "P" containing "Q," "R," "S," "T," and "U" was simultaneously translatable

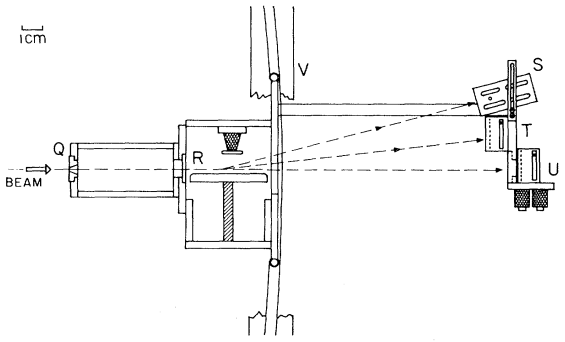

FIG. 4. Translatable detection assembly. Q: Removable circular aperture of diameter 0.025 ± 0.0025 cm; R: electrostatic charge-analyzing plates; S: positive-ion-beam monitoring Faraday-cup assembly; T: positive-ion-beam monitoring resistive-strip magnetic particle multiplier, Bendix M-306; U: neutral-beam monitoring resistive-strip magnetic particle multiplier, Bendix M-306; V: stainless-steel translation guide rail with a 238-cm radius of curvature.

and swiveled about an axis defined by the radius of curvature of the rails "V." The radius of curvature of the rails was equal to the distance 238.0 ± 0.5 cm between the rail-center and the center of the scattering target. Hence the axis of the assembly "P" pointed at and swiveled around the scattering-target "K" of Fig. 1, in contrast with our previous translatable assembly whose radius of curvature was infinite.[2]

E. Detection of fast collision products

In order to ascertain that all scattered beam components leaving the differential scattering cell were collected properly, the angular distribution of each charge component was measured at the end of the machine. The different scattered-beam charge components were selected using the electrostatic analyzer inside the translatable detector assembly of Fig. 4. Figure 5 shows some typical measured beam profiles. The maximum measured beam diameters (full width at $\frac{1}{10}$ maximum) at the end of the apparatus were 0.45 cm for the singly charged component, 0.55 cm for the neutral component, and 0.30 cm for the incident doubly charged beam. In vacuum chambers 4 and 5 we used 1.25- and 4.0-cm entrance diameters for the charged-particle ("M" and "N") and neutral-particle ("O") Faraday-cups respectively. These acceptance diameters were so much larger than the measured scattered-beam diameters at "P" that these Faraday cups doubtlessly collected every beam component completely.

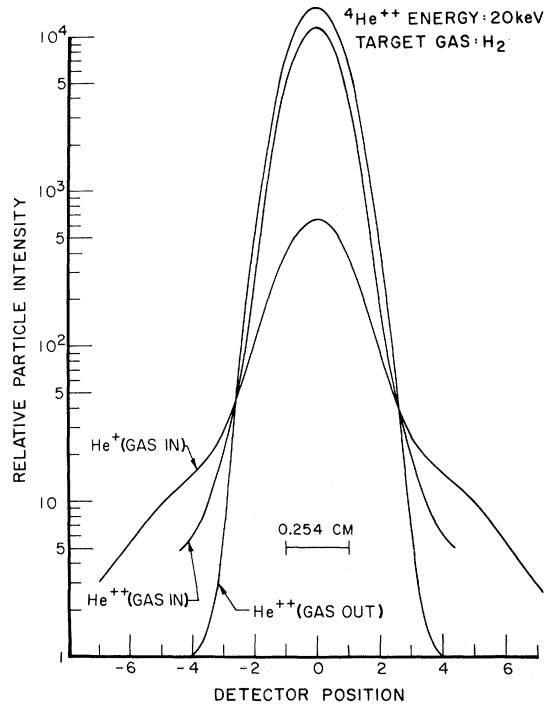

FIG. 5. Beam profile as scanned by the translatable detection assembly. The relative amplitudes are distorted slightly by reducing the He^{++} (gas in) curve by a small fraction to enhance the contrast with the He^{++} (gas out) profile. The intersection of all curves at the detector positions ± 3 bears no special significance. Each detector step ("position") was equal to 0.127-cm displacement.

The ion beams were collected at "M" and "N" with secondary-electron suppressed Faraday cups. For the neutral-atom beam at "O," the cup suppressor electrodes were reverse biased (positively) to attract the secondary-electron current. To correlate the corresponding electrometer reading with the actual rate of collection of He atoms in this cup, we used the result of Barnett and others that the ratio Δ^0/Δ^+ of secondary-electron emission coefficients for He atoms and He^+ ions is equal to 1.05 ± 0.05, independent of energy over our energy range.[11,12]

IV. RESULTS AND DISCUSSION

Appropriate specific procedures for assessing the over-all uncertainty in collision cross-section results are not well established, as systematic errors usually dominate and these can be estimated with varying degrees of conservatism. For the present measurements the long-term reproducibility of the data was generally better than ± 5%. A principal additional source of systematic error is the target-thickness measurement, where we believe the $^4He^+$-^4He reference cross section is accurate to ± 5%. In the case of our σ_{20} measurements the secondary-electron emission-coefficient ratio $\Delta^0/\Delta^+ = 1.05 \pm 0.05$ might not be quite applicable to our stainless-steel electron-emission surface, although all the available data on such ratios for keV-energy incident light ions indicates little surface dependence. On this basis we estimate an additional uncertainty of ± 10% as a best guess at the better than 80% confidence level estimated for the other sources of error. All other uncertainties are a few percent or less. As we believe our principal sources of systematic error to be uncorrelated, we generally quote an rms computed over-all uncertainty of about ±10% for values of σ_{21}, and ± 15% for values of σ_{20}, with a confidence level of 80% or higher.

Table I lists all past sources of data on keV-energy He^{++} electron-transfer cross sections. The first four references listed are for incident $^4He^{++}$ above 150 keV, where a useable beam of such ions can be prepared by the collisional stripping of $^4He^+$. The next entry at 1–8 keV was only briefly reported, with no mention of possible H_2^+ contamination. The remaining studies employed

TABLE I. Sources of data on keV-energy He^{++} electron-transfer cross sections.

Reference	Gas target	Cross sections measured	Energy range (keV)	Measurement method	Projectile mass (amu)
13	He, H_2	σ_{21}, σ_{20}	150–450	Thick target	4
14	He, Ar, N_2	σ_{21}	300–1500	Thin target	4
15	He, Ar, N_2	σ_{20}	300–1500	Thin target	4
16	He, Ar, N_2, H_2	σ_{21}, σ_{20}	300–1500	Thin target	4
17	He	σ_{21}	1–8	Thin target	4
26	He	σ_{21}, σ_{20}	15–125	Growth	3
18	N_2	σ_{21}, σ_{20}	7.7–166	Growth	3
19	He	$\sigma_{21}, \sigma_{20}, \sigma_{12}, \sigma_{10}$	1–100	Thin target	3
20	Ar, H_2	σ_{21}, σ_{20}	50–450	Growth	3
21	Ar, H_2, He, N_2, Kr, O_2	σ_{21}, σ_{20} (except for H_2)	10–60	Thin target	3

$^3He^{++}$ beams on ^4He targets and are for the range of equivalent $^4He^{++}$ energy presently studied. We observe that the greatest quantity of independent such data is available for He and N_2 targets.

The present data are presented in Figs. 6–9 and compared with that of others. The general situation is that agreement between individual investigations is often as good as ± 10%, but also that discrepancies of magnitude 20% to 35% or more often exist. Disagreement is more severe in the data for σ_{21} than for σ_{20}, a somewhat surprising situation since the latter cross sections are generally smaller and have the additional uncertainties associated with the detection of fast neutral particles.

The experimental situation with regard to values of σ_{21} is especially important, as the indicated discrepancies will shed some light on the situation

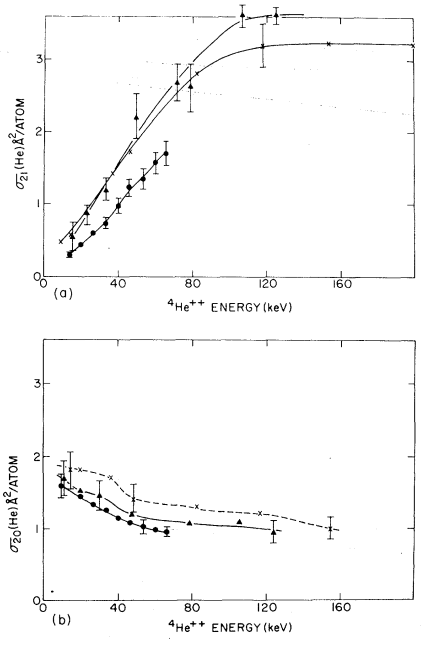

FIG. 6. (a) Experimental cross sections σ_{21}(He) for $He^{++} + He \rightarrow He^{+} + He^{+}$ collisions; (b) experimental cross sections σ_{20}(He) for $He^{++} + He \rightarrow He + He^{++}$ collisions. ▲: present data; ×: Ref. 26; ●: Ref. 21.

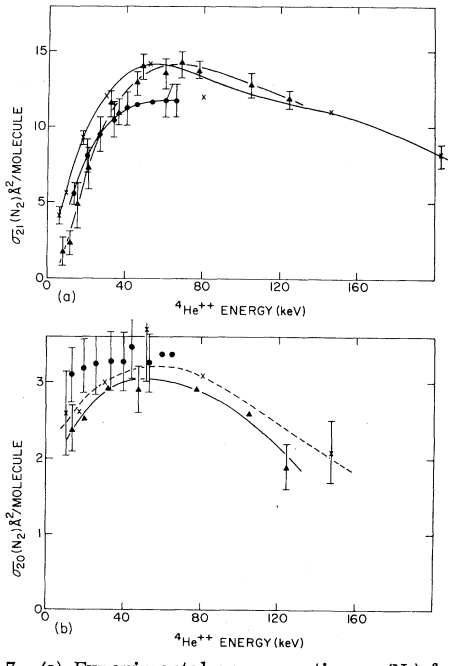

FIG. 7. (a) Experimental cross section $\sigma_{21}(N_2)$ for single electron transfer in $He^{++} + N_2$ collisions; (b) experimental cross section $\sigma_{20}(N_2)$ for double electron transfer in $He^{++} + N_2$ collisions. ▲: Present data; ×: Ref. 18; ●: Ref. 21.

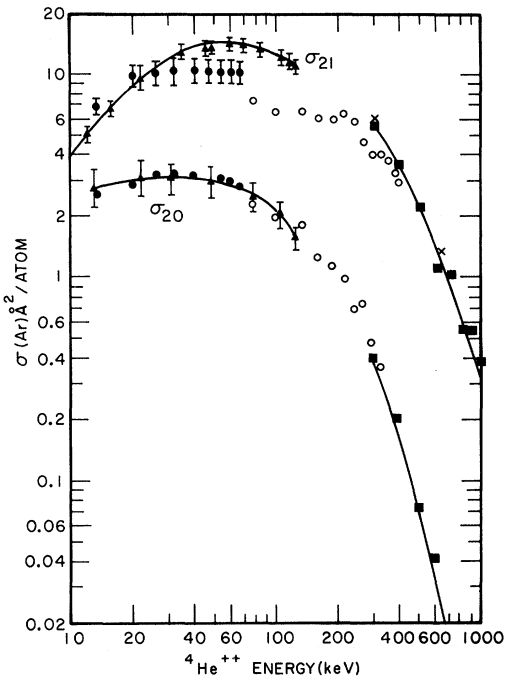

FIG. 8. Experimental cross sections for single and double electron transfer in He^{++} + Ar collisions. ▲: Present data; ●: Ref. 21; ○: Ref. 20; ■: Ref. 16; ×: Refs. 14 and 15.

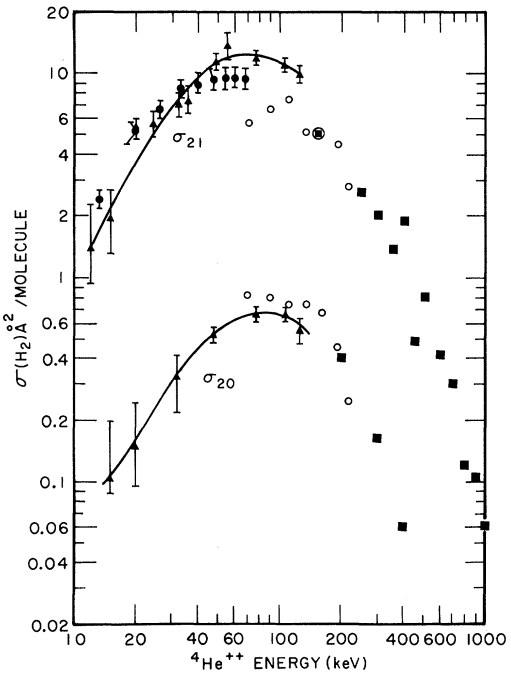

FIG. 9. Experimental cross sections for single and double electron transfer in He^{++} + H_2 collisions. ▲: present data; ●: Ref. 21; ○: Ref. 20; ■: Ref. 16.

for He^{++}-H collisions to be discussed in paper III. We observe here that for all target gases the present data at the higher energies is higher than that of Shah and Gilbody[21] (SG) by an amount 20–35%, but is in excellent agreement with that of the Berkeley group.[18,26] At the lower end of our energy range the situation is more confusing. For N_2, Ar, and H_2 gases, where σ_{21} is large, we now find the present $^4He^{++}$ values to be smaller than the $^3He^{++}$ values of SG by 20–30%, but for the small cross section σ_{21}(He) we obtain up to 55% larger values, in excellent agreement with the $^3He^{++}$ results of Berkner *et al.*[26] Lastly, our low-energy values for $\sigma_{21}(N_2)$ disagree with those of Stearns *et al.*[18] by a factor of 2.

Our conclusions are first that a standard cross section for He^{++} electron-transfer collisions can be quoted without regard to choice of isotope to perhaps ± 30%, without showing favoritism to specific experimental results. Second, a consistent discrepancy at the higher energies is that the data of Shah and Gilbody is considerably lower than that of those other investigations that obtain small amounts of scatter in the energy dependence of their cross sections.

The cross section $\sigma_{20}(H_2)$ is presently found to be unusually small at the lower energies; there exists no other data for comparison. This double-electron-transfer process is unusually interesting as the final state must involve two protons in addition to the He atom. A consideration of energy defects and the adiabatic criterion leads to the conclusion that the He atom is likely to be produced with quite high states of excitation. It would seem that this two-electron collision process would be amenable to theoretical treatment, although no such work has been done.

For the symmetrical two-electron collision system $He^{++} - He(1s^2)$, possibly important collision channels include resonant double-electron-transfer as well as a number of single-electron-transfer channels. As an initial indication of the relative importance of the various channels, we list their energy defects $\Delta E(\infty)$ at infinite internuclear separation in Table II. The two-electron-transfer process is energy resonant, and is therefore an important channel even if both electrons must be transferred in one collision. We also see that all the single-electron-transfer channels are not favored, but that, among these, processes leading to $He^+(n=2)$ or higher states may be at least as important as channel 3, producing two ground-state He^+ ions. In the lower keV-collision-energy region a molecular picture of the collision should be valid, and then channels 4 and 5, for instance, should have equal probabilities. One would expect that the calculation of a

TABLE II. Previously considered channels in $He_A^{++} + He_B(1s^2)$ collisions. The quantities $\Delta E(R_0)$ are effective energy defects approximately accounting for Coulomb repulsion in the final state (see text).

Channel	Final state	$\Delta E(\infty)$	$\Delta E(R_0)$
1. Elastic scattering	$He_A^{++} + He_B(1s^2)$	0 eV	0 eV
2. Double transfer	$He_A(1s^2) + He_B^{++}$	0 eV	0 eV
3. Single transfer into 1s	$He_A^{+}(1s) + He_B^{+}(1s)$	−29.8 eV	−19.3 eV
4. Single transfer into $n=2$	$He_A^{+}(2s, 2p_X, 2p_Z) + He_B^{+}(1s)$	+11.0 eV	+21.5 eV
5. Single transfer into 1s with $n=2$ excitation	$He_A^{+}(1s) + He_B^{+}(2s, 2p_X, 2p_Z)$	+11.0 eV	+21.5 eV
6. Single transfer into $n=3$	$He_A^{+}(3s, 3p, 3d) + He_B^{+}(1s)$	+18.5 eV	+29.0 eV
7. Single transfer into 1s with $n=3$ excitation	$He_A^{+}(1s) + He_B^{+}(3s, 3p, 3d)$	+18.5 eV	+29.0 eV
8. Single transfer into 1s with ionization	$He_A^{+}(1s) + He_B^{++} + e$	+24.6 eV	+35.1 eV

cross section for any of the single-electron-transfer channels 3–8 would need to account for the resonant channel 2, except in the high-energy limit where the short collision time does not permit two-step processes. On the other hand, at low energies the resonant process 2 should involve just its initial and final states, with coupling to the other states unimportant.

Our results for σ_{20}(He) seem to show a step near 40-keV $^4He^{++}$ energy, also observed for $^3He^{++}$ collisions near 50-keV equivalent $^4He^{++}$ energy by Berkner *et al.*[26] and predicted theoretically at 30 keV by Fulton and Mittleman.[24] This structure does not appear in the data of SG.[21] It would be of interest to know the origin of this structure.

Table III summarizes the nature of the various calculations for which results are available. The resonant cross section σ_{20}(He) is well described by two-state calculations for a wide range of energies. On the other hand, no calculations of σ_{21}(He) agree with experiment for energies below 100 keV, because a number of coupled scattering channels are involved.[28]

TABLE III. Summary of recent past calculations of $^4He^{++}$-^4He electron-transfer collision cross sections.

Reference	Type of calculation	Included channels [a]
22	Molecular basis states	1 and 2
23	Atomic basis states	1 and 2
24	Atomic basis states	1–3
25	Atomic basis states	1–5
26	High energy (OBK)	3
27	High energy (CDW)	uncoupled 3–5

[a] See Table II.

No calculations are available for He^{++} collisions with atoms or molecules more complicated than He. It is of interest to see how the energy defects for the various collision channels change as one passes from the atypical target atom He with its unusually large first and second ionization potentials to a more typical target atom such as Ar, as is shown in Table IV. Now single-electron transfer into excited states is fractionally more favored than for an He target atom, and double electron transfer forming the ground state of He is favorable only when an additional electron in the remanent Ar^{++} ion can be considerably excited.

We observe that maxima in the energy dependences of σ_{21} for Ar, N_2, and H_2 occur at almost the same energy, 60–70 keV, values considerably lower than that for σ_{21}(He). This is qualitatively consistent with electron transfer into excited states and the unmodified adiabatic criterion. The energies E_m of the maxima σ_m predicted in this

TABLE IV. Energy defects in He^{++}-Ar collisions.

Final state	$\Delta E(\infty)$	$\Delta E(R_0)$
$He^{+}(1s) + Ar^{+}(3s^2 3p^5)$	−38.6 eV	−36.9 eV
$He^{+}(n=2) + Ar^{+}(3s^2 3p^5)$	+2.2 eV	+3.9 eV
$He^{+}(n=3) + Ar^{+}(3s^2 3p^5)$	+9.7 eV	+11.4 eV
$He^{+}(1s) + Ar^{++}(3p^4) + e$	−11.0 eV	−9.3 eV
$He(1s^2) + Ar^{++}(3p^4)$	−35.6 eV	−35.6 eV
$He(1s, n=2) + Ar^{++}(3p^4)$	−13.9 eV	−13.9 eV
$He(1s^2) + Ar^{++}(3s^2, 3p^3, 5s)$	−4.3 eV	−4.3 eV

way are

	E_m(He)	E_m(Ar)
$n=1$	0.53 MeV	0.88 MeV
$n=2$	72 keV	2.9 keV
$n=3$	0.20 MeV	56 keV

As the simple first ionization potentials of Ar, N_2, and H_2 are 15.76, 15.58, and 15.42 eV, respectively, we expect the situation for N_2 and H_2 to be similar to that for Ar. We point out that the reason these $n \neq 1$ E_m values are much lower than expected is because the energy defect for the collision should not be chosen at infinite nuclear separation R, but rather at some finite $R = R_0$ where the dynamic coupling between the relevant (molecular) states equals the total dynamic splitting of those states. For the present He^{++} single-electron processes a long-range Coulomb repulsion is present in the final state but absent in the initial states; the difference is a major contribution to the energy defect $\Delta E(R)$ at R_0. For the present processes $\Delta E(R_0) > \Delta E(\infty)$, and hence E_m values are at higher energies than those listed immediately above.

A rough estimate of R_0 can be obtained by setting $\sigma_m = \frac{1}{2}\pi R_0^2$, which gives $R_0 \sim 1.4$ Å for He and $R_0 \sim 9$ Å for the other gases. Adding $1/R_0$ a.u. of energy to $\Delta E(\infty)$ gives the values of $\Delta E(R_0)$ listed in Tables II and IV with corresponding new values for $E_m = E_m^c$:

	E_m^c(He)	E_m^c(Ar)
$n=1$	0.22 MeV	0.81 MeV
$n=2$	0.27 MeV	9.0 keV
$n=3$	0.50 MeV	77.2 keV

Agreement with experiment is now a little better. We note that our simple correction for the Coulomb repulsion does not alter the conclusion that electron transfer into excited states dominates σ_{21} for Ar, N_2 and H_2. However, we no longer can say this for σ_{21}(He), as direct production of $He^+(1s)$ now seems comparable. Further theoretical work for $He^{++} - He$ is especially desirable, as is experimental study of the fractional population of the different final states of He^+.

†Work sponsored by the U. S. Air Force Office of Scientific Research, AFSC, under AFOSR Contract No. F44620-71-C-0042.

[1]J. E. Bayfield and G. A. Khayrallah, *Proceedings of the Eight ICPEAC* (Institute of Physics, Belgrade, 1973), p. 782.
[2]J. E. Bayfield, Phys. Rev. 182, 115 (1969).
[3]R. N. Il'in, B. I. Kikiani, V. A. Oparin, E. S. Solov'ev, and N. V. Fedorenko, Zh. Eksp. Teor. Fiz. 46, 1208 (1964) [Sov. Phys.—JETP 19, 817 (1964)].
[4]J. Ero, Nucl. Instrum. Methods 3, 303 (1958).
[5]P. E. Vorotnikov, Yu. G. Zubov, and Yu. D. Malchanov, Prib. Tekh. Eksp. 5, 33 (1966) [Instrum. Exp. Tech. 9, 1051 (1966)].
[6]C. F. Barnett and P. M. Stiers, Phys. Rev. 109, 385 (1958).
[7]V. M. Dukelskii, V. V. Afrosimov, and N. V. Fedorenko, Zh. Eksp. Teor. Fiz. 30, 792 (1956) [Sov. Phys.—JETP 3, 764 (1956)].
[8]F. J. Deheer, J. Schutten, and H. Moustafa, Physica (Utr.) 32, 1793 (1966).
[9]H. B. Gilbody, K. F. Dunn, R. Browning, and C. J. Latimer, J. Phys. B 4, 800 (1971).
[10]J. E. Bayfield, Phys. Rev. 185, 105 (1969).
[11]C. F. Barnett, Phys. Rev. 96, 973 (1954).
[12]U. A. Arifov, *Interaction of Atomic Particles with a Solid Surface* (Consultants Bureau, New York, 1969), p. 172.
[13]S. K. Allison, Phys. Rev. 109, 76 (1958).
[14]V. S. Nikolaev, I. S. Dimitriev, L. N. Fateeva, and Ya. A. Teplova, Zh. Eksp. Teor. Fiz. 40, 989 (1961) [Sov. Phys.—JETP 13, 695 (1961)].
[15]V. S. Nikolaev, L. N. Fateeva, I. S. Dimitriev, and Ya. A. Teplova, Zh. Eksp. Teor. Fiz. 41, 89 (1962) [Sov. Phys.—JETP 14, 67 (1962)].
[16]L. I. Pivovar, M. T. Novikov, and V. M. Tubaev, Zh. Eksp. Teor. Fiz. 42, 1490 (1962) [Sov. Phys.—JETP 15, 1035 (1962)].
[17]G. R. Hertel and W. S. Koski, J. Chem. Phys. 40, 3452 (1964).
[18]J. W. Stearns, K. H. Berkner, V. J. Honey, and R. V. Pyle, Phys. Rev. 166, 40 (1968).
[19]V. V. Afrosimov, G. A. Lieko, Yu. A. Mamaev, and N. N. Panov, in Ref. 1, p. 175.
[20]R. A. Baragiola and I. B. Nemirovsky, Nucl. Instrum. Methods 110, 511 (1973).
[21]M. B. Shah and H. B. Gilbody, J. Phys. B 7, 256 (1974).
[22]A. F. Ferguson and B. L. Moiseiwitsch, Proc. Phys. Soc. Lond. 74, 457 (1959).
[23]D. Basu, S. C. Mukherjee, and N. C. Sil, in *Atomic Collision Processes*, edited by M. R. C. McDowell (North-Holland, Amsterdam, 1964), p. 769.
[24]M. J. Fulton and M. H. Mittleman, Proc. Phys. Soc. Lond. 87, 669 (1966).
[25]S. C. Mukherjee, K. Roy, and N. C. Sil, J. Phys. B 6, 467 (1973).
[26]K. H. Berkner, R. V. Pyle, J. W. Stearns, and J. C. Warren, Phys. Rev. 166, 44 (1968).
[27]D. S. Belkic and R. K. Janev, J. Phys. B 6, 1020 (1973).
[28]For a graphical comparison of theory and experiment see J. E. Bayfield, in *Atomic Physics IV*, edited by G. zu Putlitz, E. W. Weber, and A. Winnacker (Plenum, New York, 1974), Figs. 20 and 21.